行政院國家科學委員會補助專題研究計畫 ■ 成果報告 □期中進度報告

壓電螺旋差排與含任意形狀雙層異質之三相複合材料之交互作用分析

計畫類別：■ 個別型計畫 □ 整合型計畫
計畫編號：NSC 99-2221-E-252-005
執行期間： 99 年 8 月 1 日至 100 年 7 月 31 日

計畫主持人：沈明河 南開技術學院自動化工程系
共同主持人：洪仕育 南開技術學院自動化工程系
計畫參與人員：兼任助理 李恩冠、柯凱琦

成果報告類型(依經費核定清單規定繳交)：■精簡報告 □完整報告

本成果報告包括以下應繳交之附件：
□赴國外出差或研習心得報告一份
□赴大陸地區出差或研習心得報告一份
□出席國際學術會議心得報告及發表之論文各一份
□國際合作研究計畫國外研究報告書一份

處理方式：除產學合作研究計畫、提升產業技術及人才培育研究計畫、列管計畫及下列情形者外，得立即公開查詢
□涉及專利或其他智慧財產權，□一年■二年後可公開查詢

執行單位：南開技術學院自動化工程系

中 華 民 國 100 年 7 月 31 日

行政院國家科學委員會專題研究計畫成果報告

壓電螺旋差排與含任意形狀雙層異質之三相複合材料之交互作用分析

A piezoelectric screw dislocation interacting with an arbitrarily shaped three-phase composite

計畫編號：NSC 99-2221-E-252-005

執行期限：99 年 8 月 1 日至 100 年 7 月 31 日

主持人：沈明河　南開科技大學自動化工程系

共同主持人：洪仕育　南開科技大學自動化工程系

計畫參與人員：兼任助理 李恩冠、柯凱琦

中文摘要

本計畫主要探討壓電螺旋差排與含任意形狀雙層異質之三相複合材料受平面電場及反平面彈性位移場作用下之交互作用分析。藉由複變函數法、保角轉換、Faber 級數、和勞倫斯級數，我們可以將三相複合材料各區域內解析之壓電應力函數表示成含待定係數之級數式。而這些待定係數可由邊界連續條件組成之一組線性方程式，再由數值方法求解此待定係數。當壓電應力函數之各係數求得之後，各區域之應力場，電場及映射力等均可以顯解的方式明確地表示出來。最後，我們將提供各種數值計算結果，用以探討各材料組成及幾何形狀等對邊界應力，邊界電場及映射力之影響。這些研究結果除可應用於壓電材料之感測器及驅動器等領域中，用以選用適當複合材料以期增加感測器之靈敏度，達到較佳之輸出特性，亦可作為分析三相任意形狀複合材料料含裂縫問題之基礎函數(Green's function)。

關鍵詞：壓電材料；任意形狀異質；螺旋差排；Faber 級數

Abstract

This project investigated the interaction of a piezoelectric screw dislocation with an arbitrarily shaped three-phase composite subjected to remote anti-plane shear and electric fields. Based on the methods of complex variable, conformal mapping, Faber series and Laurent series, the analytical complex potentials for all three regions can be expressed in series form with unknown coefficients. The continuity conditions of the interfaces are used to build up a set of linear equations to determine the unknown coefficients. After the unknown coefficients are solved, the stress, electric field and image force can be expressed explicitly. Numerical results will provide to show the effect of the inclusion shape, the material combinations on the electro-elastic fields and image force calculated through the generalized Peach-Koehler formula. The solutions proposed here can be served as kernel functions to analyze the corresponding piezoelectric cracking problems.

Keywords: Piezoelectric material, Arbitrarily shaped inclusion, Screw dislocation, Faber series

1. Introduction

Due to the capability of the transfer between mechanical and electric energy, piezoelectric materials are used extensively in electromechanical devices such as actuators, sensors, and transducers. During the manufacture process, piezoelectric ceramics are brittle and likely to generate micro-defects such as dislocations, micro-cracks, cavities, inclusions, etc. The existences of various defects cause geometric discontinuities and induce high stress concentrations, which may greatly influence the performance of piezoelectric devices. Therefore, the mechanical stress analysis of piezoelectric materials with defects plays an important role in understanding the behavior and the performance of these devices. Pak (1992) investigated a circular piezoelectric inclusion embedded in an infinite piezoelectric matrix. Meguid and Zhong

(1998) studied the elliptical inhomogeneity problem in piezoelectric materials under antiplane shear and inplane electric field. Chao and Chang (1999) investigated the interaction of circular inclusions in antiplane piezoelectricity. Zhang and Tong (1996) formulated the mechanical and electric fields in a piezoelectric material around an elliptical cylinder cavity and the electric field within the cavity. The three-phase model is quite important in composite mechanics research. Jiang and Cheung (2001) proposed a three-phase piezoelectric cylinder model and gave an exact solution by using the Laurent expansion technique, but their result is based on a uniform far-field loading condition. Jiang et al. (2001) proposed a three-phase piezoelectric confocal elliptical cylinder model and obtained the solution for the model subjected to antiplane mechanical and inplane electric load at infinity by using the conformal mapping integrated with the Laurent series expansion technique. Sudak (2003) proposed a three-phase inclusion model and investigated the influence of the interphase layer on the electroelastic fields. The fundamental solutions for a point dislocation and a concentrated force play another significant role in the analysis of many problems. Dislocation solutions can be served as kernel functions for general crack problems, such as crack deflections, kink cracks, crack/inclusion interactions, etc. As a result, a considerable amount of attention has been paid to discuss the effects of a point load. The first studies of dislocation fields in piezoelectrics were accomplished by Kosevich et al. (1968) and Saada (1971). They extended the exact plane-strain solution for a straight dislocation in anisotropic purely elastic medium to include the complete piezoelectric coupling into the constitutive equations. Barnett and Lothe (1975) extended the six-dimensional Stroh formalism to eight-dimensional formalism for solving the problem of a line dislocation and a line charge in anisotropic piezoelectric materials. Nowacki and Alshits (2007) used a 4D variant of this formalism for a description of electroelastic fields of arbitrary curved dislocations in unbounded piezoelectric media of unrestricted anisotropy. Pak (1990) considered a screw dislocation in a material and derived the generalized Peach-Koehler force acting on a screw dislocation. Kattis el al. (1998) investigated the electroelastic interaction effects of a piezoelectric screw dislocation interacting with circular inclusion in piezoelectric material. Meguid and Deng (1998) and Deng and Meguid (1999) discussed the electro-elastic interaction between a screw dislocation and an elliptical inhomogeneity in piezoelectric material. Lee et al. (2000) discussed the interaction between a semi-infinite crack and a screw dislocation under antiplane mechanical and inplane electrical loadings in a linear piezoelectric material. Huang and Kuang (2001) evaluated the generalized electromechanical force when the dislocation locates inside, outside or on the interface of the elliptical inhomogeneity in an infinite piezoelectric medium. Liu et al. (2004) dealt with the interaction of a piezoelectric screw dislocation with an interphase layer between the circular inclusion and the piezoelectric matrix.

For the case of various shaped defects, the solution of an infinite plate with an arbitrarily shaped rigid inclusion or an arbitrarily shaped hole can be obtained by use of the conformal mapping. The in-plane tension and anti-plane bending of a thin plate containing a rigid polygonal inclusion and a hole in an elastic matrix were studied by Gdoutos and Kattis (1990) and Pengfei and Ishikawa (1995) with conformal mapping carried out by an infinite power series. Based on the complex variable and analytical continuation method, Shen et al. (2009) studied the piezoelectric problems for a coated hole of quasi-polygonal shape embedded in an infinite matrix subjected to electromechanical loadings. However, there are only a few papers dealing with the problem of a plate with an arbitrarily shaped inclusion, because the mapping function in the region of inclusion is too complicated. Based on the assumption that the inclusion and matrix have the same elastic constant, Ru (1999; 2000) developed a method for solving the arbitrarily shaped inclusion problems in elastic media and piezoelectric media. Wang and Shen (2003) used the same method to obtain the analytical solutions for the problem of inclusions of arbitrary shape in magnetoelectroelastic composites. Recently, Gao and Noda (2004) developed a successful approach based on the Faber series method to investigate the anti-plane problem of an arbitrarily shaped piezoelectric inclusion embedded in an infinite piezoelectric medium. By means of complex variable methods and Faber series expansion, Wang and Sudak (2006) investigated the interaction between a screw dislocation and an arbitrary shaped elastic inhomogeneity with different material properties than the surrounding matrix. To our knowledge, the interaction between a screw dislocation and coated inclusion of arbitrary shape has not been recorded in the literature. This work is using the Faber series method to obtain the Green's function for a three-phase arbitrarily shaped piezoelectric composite.

2. Basic equations

In a fixed rectangular coordinates system (x_1, x_2, x_3), the basic equations for linear piezoelectric materials can be written as

$$\tau_{ij,j} = 0 \tag{1}$$

$$D_{i,i} = 0 \tag{2}$$

$$\gamma_{ij} = \frac{1}{2}(u_{i,j} + u_{j,i}) \tag{3}$$

$$E_i = -\varphi_{,i} \tag{4}$$

$$\tau_{ij} = c_{ijkl}\gamma_{kl} - e_{kij}E_j \tag{5}$$

$$D_i = e_{ikl}\gamma_{kl} + \varepsilon_{ik}E_k \tag{6}$$

where the repeated indices mean summation and a comma stands for partial differentiation. c_{ijkl} , e_{kij} and ε_{ik} are the corresponding elastic, piezoelectric and dielectric constants, respectively. τ_{ij} , u_i , D_i , φ , γ_{ij} and E_i are stress, displacement, electric displacement, electric potential, strain and electric field, respectively. Since the symmetry of the stress and strain tensor, and since the stress-strain relation in linear elasticity can be derived from a strain energy density function, the material constants satisfy the following symmetric relation:

$$c_{ijkl} = c_{klij} = c_{ijlk} = c_{jikl}, \quad e_{kij} = e_{kji}, \quad \varepsilon_{ik} = \varepsilon_{ki}$$

2.1. Anti-plane deformation

In this paper, we consider a coated inclusion of arbitrary shape embedded in an infinite matrix subjected to anti-plane mechanical and in-plane electrical loadings (see Fig. 1). The matrix and the coated inclusion are assumed to be transversely isotropic and poled in the x_3 direction. The anti-plane deformation is determined by the out-of-plane displacement u_3 and the in-plane electric potential ϕ, and both are functions of x_1 and x_2 only, such that

$$u_1 = u_2 = 0, \quad u_3 = u_3(x_1, x_2), \quad \phi = \phi(x_1, x_2)$$

The governing equations (1) and (2) can be simplified to

$$c_{44}\nabla^2 u_3 - e_{15}\nabla^2\phi = 0 \tag{7}$$

$$e_{15}\nabla^2 u_3 - \varepsilon_{11}\nabla^2\phi = 0 \tag{8}$$

where $\nabla^2 = \frac{\partial^2}{\partial x_1^2} + \frac{\partial^2}{\partial x_2^2}$ is the two-dimensional Laplace operator.

In order to formulate the interface boundary condition, it is convenient to use a complex representation for u_3 and ϕ which are grouped as a vector

$$\mathrm{Re}[\mathbf{U}(z)] = \begin{Bmatrix} u_3 \\ \phi \end{Bmatrix} \tag{9}$$

where Re denotes the real part of a complex function and $\mathbf{U}(z)$ is the complex generalized displacement with two components being analytic functions. The components of the stress, electric displacement, stain and electric field are related to the generalized displacement by

$$\begin{Bmatrix} \tau_{31} - i\tau_{32} \\ D_1 - iD_2 \end{Bmatrix} = \begin{bmatrix} c_{44} & e_{15} \\ e_{15} & -\varepsilon_{11} \end{bmatrix} \mathbf{U}'(z) = \mathbf{CU}'(z) \tag{10}$$

$$\begin{Bmatrix} \gamma_{31} - i\gamma_{32} \\ -E_1 + iE_2 \end{Bmatrix} = \mathbf{U}'(z) \tag{11}$$

In order to express the boundary condition in terms of $\mathbf{U}(z)$ rather than its derivative $\mathbf{U}^{'}(z)$, we take an integration of the traction t and normal electric displacement D_n as

$$\int \begin{Bmatrix} t \\ D_n \end{Bmatrix} ds = \mathrm{Im}\left[\mathbf{CU}(z)\right] \tag{12}$$

where $\left[t \quad D_n\right]^T$ is referred to as the generalized traction and Im denotes the imaginary part of a complex function.

2.2. Conformal mapping

We introduce a mapping function as in England (1971)

$$z = \Omega(\zeta) = R\left(\zeta + \sum_{n=1}^{\infty} m_n \zeta^{-n}\right) \tag{13}$$

where m_n are the constants corresponding to the power of ζ in the mapping function for a given shape of inclusion. R is a constant for size of inclusion. Substituting $\zeta = \rho e^{i\eta}$ ($\rho \geq 1$) into Eq. (13), it becomes

$$z = \Omega(\zeta) = R\left[\rho\cos\eta + \sum_{n=1}^{\infty} \frac{m_n}{\rho^n}\cos n\eta + i(\rho\sin\eta - \sum_{n=1}^{\infty} \frac{m_n}{\rho^n}\sin n\eta)\right]$$

This mapping function will map the smooth contours Γ_a and Γ_b in the z-plane onto the concentric circles L_a and L_b with radii $\rho_a = 1$ and $\rho_b > 1$ in the ζ-plane. It also transforms the region of matrix Ω_c and the interface layer Ω_b in the z-plane into the exterior region S_c and the annular region S_b in the ζ-plane (see Fig. 2).

3. General solution

3.1. Series forms of complex potentials $\mathbf{U}_a(z)$, $\mathbf{U}_b(\zeta)$ *and* $\mathbf{U}_c(\zeta)$

The complex potential $\mathbf{U}_a(z)$ which is analytical in the region Ω_a, can be expanded as a Faber series and expressed as follows

$$\mathbf{U}_a(z)=\sum_{k=1}^{\infty}\mathbf{a}_k P_k(z) \qquad z\in\Omega_a \tag{14}$$

where $\mathbf{a}_k$ are unknown coefficient vectors to be determined and $P_k(z)$ are the k-th degree Faber polynomials which have the following form

$$P_k(z)=\zeta^k+\sum_{n=1}^{\infty}\beta_{k,n}\zeta^{-n} \tag{15}$$

, and the coefficients $\beta_{k,n}$ can be determined by the following recurrence relations [Gao and Noda (2004)]

$$\begin{aligned}&\beta_{1,n}=m_n\\&\beta_{k+1,n}=m_{k+n}+\beta_{k,n+1}+\sum_{i=1}^{n}m_{n-i}\beta_{k,i}-\sum_{i=1}^{k}m_{k-i}\beta_{i,n},\ (k,n=1,2,3\dots)\end{aligned} \tag{16}$$

Substituting Eq. (16) into Eq. (15) yields

$$\mathbf{U}_a(\zeta)=\sum_{n=1}^{\infty}\mathbf{a}_n\zeta^n+\sum_{n=1}^{\infty}\left(\sum_{k=1}^{\infty}\mathbf{a}_k\beta_{k,n}\right)\zeta^{-n} \tag{17}$$

The other complex potentials $\mathbf{U}_b(\zeta)$, $\mathbf{U}_c(\zeta)$ which are analytical in the regions $|\zeta|\ge\rho_a$, $|\zeta|\le\rho_b$ and $|\zeta|\ge\rho_b$, respectively, can be represented by the Lautent series

$$\mathbf{U}_b(\zeta)=\sum_{n=1}^{\infty}\mathbf{b}_n\zeta^n+\mathbf{b}_{-n}\zeta^{-n} \tag{18}$$

$$\mathbf{U}_c(\zeta)=\sum_{n=1}^{\infty}\mathbf{c}_{-n}\zeta^{-n} \tag{19}$$

where $\mathbf{b}_n$, $\mathbf{b}_{-n}$ and $\mathbf{c}_{-n}$ are unknown coefficient vectors to be determined.

3.2. Boundary conditions

The assumption of perfect bonding of the three-phase composite implies the continuities of generalized displacement and traction across the interfaces, which lead to the following conditions.

$$\mathrm{Re}[\mathbf{U}_a(\sigma)]=\mathrm{Re}[\mathbf{U}_b(\sigma)] \qquad \sigma\in L_a \tag{20}$$

$$\mathrm{Im}[\mathbf{C}_a\mathbf{U}_a(\sigma)]=\mathrm{Im}[\mathbf{C}_b\mathbf{U}_b(\sigma)] \qquad \sigma\in L_a \tag{21}$$

$$\mathrm{Re}[\mathbf{U}_b(\sigma)]=\mathrm{Re}[\mathbf{U}_c(\sigma)+\mathbf{U}_0(\sigma)] \qquad \sigma\in L_b \tag{22}$$

$$\mathrm{Im}[\mathbf{C}_b\mathbf{U}_b(\sigma)]=\mathrm{Im}[\mathbf{C}_c\mathbf{U}_c(\sigma)+\mathbf{C}_c\mathbf{U}_0(\sigma)] \qquad \sigma\in L_b \tag{23}$$

where

$$\mathbf{C}_a=\begin{bmatrix} c_{44}^a & e_{15}^a \\ e_{15}^a & -\varepsilon_{11}^a \end{bmatrix},\ \mathbf{C}_b=\begin{bmatrix} c_{44}^b & e_{15}^b \\ e_{15}^b & -\varepsilon_{11}^b \end{bmatrix},\ \mathbf{C}_c=\begin{bmatrix} c_{44}^c & e_{15}^c \\ e_{15}^c & -\varepsilon_{11}^c \end{bmatrix}$$

, and $\mathbf{U}_0(\zeta)$ represents the solution corresponding to the homogeneous medium. Suppose a screw dislocation with Burgers vector b_z and electric potential jump $\Delta\phi$ located at the point $\zeta=\zeta_0$ which is subjected to a point force p_0 and a point charge q_0. The solution of the corresponding homogeneous problem can be expressed as

$$\mathbf{U}_0(\zeta)=\frac{1}{2\pi}\begin{bmatrix} \dfrac{-\varepsilon_{11}p_0+e_{15}q_0}{c_{44}\varepsilon_{11}+e_{15}^2}-b_z i \\ -\dfrac{e_{15}p_0+c_{44}q_0}{c_{44}\varepsilon_{11}+e_{15}^2}-\Delta\phi i \end{bmatrix}\log(\zeta-\zeta_0)$$

where $\mathbf{U}_0(\zeta)$ is analytical in the whole plane except the points of branch cut, and have the characteristic as follows

$$\mathrm{Re}[\oint_{\zeta_0}\mathbf{U}_0'(\zeta)d\zeta]=\begin{bmatrix} b_z \\ \Delta\phi \end{bmatrix},\quad \mathrm{Im}[\oint_{\zeta_0}\mathbf{C}\mathbf{U}_0'(\zeta)d\zeta]=\begin{bmatrix} -p_0 \\ q_0 \end{bmatrix}$$

Since $\mathbf{U}_0(\zeta)$ is holomorphic in the region $|\zeta|<|\zeta_0|$, it can be expanded as

$$\mathbf{U}_0(\zeta)=\sum_{n=1}^{\infty}\mathbf{d}_n\zeta^n \tag{24}$$

With the aid of the following relation

$$\log(1-\zeta)=-\sum_{n=1}^{\infty}\frac{\zeta^n}{n},\qquad |\zeta|<1 \tag{26}$$

, the coefficient vectors $\mathbf{d}_n$ are given as follows

$$\mathbf{d}_n=\frac{-\zeta_0^{-n}}{2\pi n}\begin{bmatrix} \dfrac{-\varepsilon_{11}p_0+e_{15}q_0}{c_{44}\varepsilon_{11}+e_{15}^2}-b_z i \\ -\dfrac{e_{15}p_0+c_{44}q_0}{c_{44}\varepsilon_{11}+e_{15}^2}-\Delta\phi i \end{bmatrix} \tag{27}$$

3.3. Determinations of $\mathbf{U}_a(\zeta)$, $\mathbf{U}_b(\zeta)$ *and* $\mathbf{U}_c(\zeta)$

Substituting the series expression of complex potentials $\mathbf{U}_a(\zeta)$, $\mathbf{U}_b(\zeta)$, $\mathbf{U}_c(\zeta)$ and $\mathbf{U}_0(\zeta)$, as in Eqs. (17), (18) (19) and (24) into the boundary conditions (20)-(23), and equaling the coefficients of σ^n ($n\geq 1$), yields

$$\mathbf{a}_n+\sum_{k=1}^{\infty}\bar{\mathbf{a}}_k\bar{\beta}_{k,n}=\mathbf{b}_n+\bar{\mathbf{b}}_{-n} \tag{28}$$

$$\mathbf{C}_a\left\{\mathbf{a}_n-\sum_{k=1}^{\infty}\bar{\mathbf{a}}_k\bar{\beta}_{k,n}\right\}=\mathbf{C}_b\left\{\mathbf{b}_n-\bar{\mathbf{b}}_{-n}\right\} \tag{29}$$

$$\mathbf{b}_n + \frac{\bar{\mathbf{b}}_{-n}}{\rho^{2n}} = \mathbf{d}_n + \frac{\bar{\mathbf{c}}_{-n}}{\rho^{2n}} \tag{30}$$

$$\mathbf{C}_b \left\{ \mathbf{b}_n - \frac{\bar{\mathbf{b}}_{-n}}{\rho^{2n}} \right\} = \mathbf{C}_c \left\{ \mathbf{d}_n - \frac{\bar{\mathbf{c}}_{-n}}{\rho^{2n}} \right\} \tag{31}$$

Decoupling of Eqs. (28)-(31) yields

$$\begin{aligned}&[(1+\frac{1}{\rho^{2n}})(\mathbf{I}+\mathbf{C}_c^{-1}\mathbf{C}_a)+(1-\frac{1}{\rho^{2n}})(\mathbf{C}_b^{-1}\mathbf{C}_a+\mathbf{C}_c^{-1}\mathbf{C}_b)]\mathbf{a}_n + \\ &[(1+\frac{1}{\rho^{2n}})(\mathbf{I}-\mathbf{C}_c^{-1}\mathbf{C}_a)+(1-\frac{1}{\rho^{2n}})(\mathbf{C}_c^{-1}\mathbf{C}_b-\mathbf{C}_b^{-1}\mathbf{C}_a)]\sum_{k=1}^{\infty}\bar{\mathbf{a}}_k\bar{\beta}_{k,n} = 4\mathbf{d}_n\end{aligned} \tag{32}$$

Taking the conjugate of Eq. (32) leads to

$$\begin{aligned}&[(1+\frac{1}{\rho^{2n}})(\mathbf{I}+\mathbf{C}_c^{-1}\mathbf{C}_a)+(1-\frac{1}{\rho^{2n}})(\mathbf{C}_b^{-1}\mathbf{C}_a+\mathbf{C}_c^{-1}\mathbf{C}_b)]\bar{\mathbf{a}}_n + \\ &[(1+\frac{1}{\rho^{2n}})(\mathbf{I}-\mathbf{C}_c^{-1}\mathbf{C}_a)+(1-\frac{1}{\rho^{2n}})(\mathbf{C}_c^{-1}\mathbf{C}_b-\mathbf{C}_b^{-1}\mathbf{C}_a)]\sum_{k=1}^{\infty}\mathbf{a}_k\beta_{k,n} = 4\bar{\mathbf{d}}_n\end{aligned} \tag{33}$$

Truncating the above infinite system of linear algebraic equations at a large N terms, Eqs. (32) and (33) constitute a system of $2N$ linear equations to determine the $2N$ unknown coefficient vectors $\mathbf{a}_n$ and $\bar{\mathbf{a}}_n$. After $\mathbf{a}_n$ are found the other unknown coefficient vectors $\mathbf{b}_n$, $\mathbf{b}_{-n}$ and $\mathbf{c}_{-n}$ can be easily found by the relations of Eqs. (28)-(31).

3.4. Stress and electric field

Once the complex potential for each component is determined, the stress and electric field of each component can be easily found from Eqs. (10) and (11).

$$\begin{Bmatrix}\tau_{31}-i\tau_{32}\\ D_1-iD_2\end{Bmatrix} = \mathbf{C}_a \frac{\sum_{n=1}^{\infty} n\left[\mathbf{a}_n\zeta^{n-1} - \left(\sum_{k=1}^{\infty}\mathbf{a}_k\beta_{k,n}\right)\zeta^{-n-1}\right]}{R\left(1-\sum_{n=1}^{\infty}m_n n\zeta^{-n-1}\right)} \qquad z\in\Omega_a \tag{34}$$

$$\begin{Bmatrix}\gamma_{31}-i\gamma_{32}\\ -E_1+iE_2\end{Bmatrix} = \frac{\sum_{n=1}^{\infty} n\left[\mathbf{a}_n\zeta^{n-1} - \left(\sum_{k=1}^{\infty}\mathbf{a}_k\beta_{k,n}\right)\zeta^{-n-1}\right]}{R\left(1-\sum_{n=1}^{\infty}m_n n\zeta^{-n-1}\right)} \qquad z\in\Omega_a \tag{35}$$

$$\begin{Bmatrix}\tau_{31}-i\tau_{32}\\ D_1-iD_2\end{Bmatrix} = \mathbf{C}_b \frac{\sum_{n=1}^{\infty} n\left[\mathbf{b}_n\zeta^{n-1} - \mathbf{b}_{-n}\zeta^{-n-1}\right]}{R\left(1-\sum_{n=1}^{\infty}m_n n\zeta^{-n-1}\right)} \qquad \zeta\in S_b \tag{36}$$

$$\begin{Bmatrix}\gamma_{31}-i\gamma_{32}\\ -E_1+iE_2\end{Bmatrix} = \frac{\sum_{n=1}^{\infty} n\left[\mathbf{b}_n\zeta^{n-1} - \mathbf{b}_{-n}\zeta^{-n-1}\right]}{R\left(1-\sum_{n=1}^{\infty}m_n n\zeta^{-n-1}\right)} \qquad \zeta\in S_b \tag{37}$$

$$\begin{Bmatrix} \tau_{31} - i\tau_{32} \\ D_1 - iD_2 \end{Bmatrix} = \mathbf{C}_c \frac{-\sum_{n=1}^{\infty} n\mathbf{c}_{-n}\zeta^{-n-1} + \frac{1}{2\pi}\begin{bmatrix} \frac{-\varepsilon_{11}p_0 + e_{15}q_0}{c_{44}\varepsilon_{11} + e_{15}^2} - bi \\ -\frac{e_{15}p_0 + c_{44}q_0}{c_{44}\varepsilon_{11} + e_{15}^2} - \Delta\phi i \end{bmatrix}\frac{1}{\zeta - \zeta_0}}{R\left(1 - \sum_{n=1}^{\infty} m_n n\zeta^{-n-1}\right)} \qquad \zeta \in S_c \tag{38}$$

$$\begin{Bmatrix} \gamma_{31} - i\gamma_{32} \\ -E_1 + iE_2 \end{Bmatrix} = \frac{-\sum_{n=1}^{\infty} n\mathbf{c}_{-n}\zeta^{-n-1} + \frac{1}{2\pi}\begin{bmatrix} \frac{-\varepsilon_{11}p_0 + e_{15}q_0}{c_{44}\varepsilon_{11} + e_{15}^2} - bi \\ -\frac{e_{15}p_0 + c_{44}q_0}{c_{44}\varepsilon_{11} + e_{15}^2} - \Delta\phi i \end{bmatrix}\frac{1}{\zeta - \zeta_0}}{R\left(1 - \sum_{n=1}^{\infty} m_n n\zeta^{-n-1}\right)} \qquad \zeta \in S_c \tag{39}$$

The normal and tangential components of the stress, electric displacement, strain and electric field along the interfaces can be expressed as

$$\begin{Bmatrix} \tau_{3n} - i\tau_{3t} \\ D_n - iD_t \end{Bmatrix} = \begin{Bmatrix} \tau_{31} - i\tau_{32} \\ D_1 - iD_2 \end{Bmatrix} e^{i\alpha} \tag{40}$$

$$\begin{Bmatrix} \gamma_{3n} - i\gamma_{3t} \\ -E_n + iE_t \end{Bmatrix} = \begin{Bmatrix} \gamma_{31} - i\gamma_{32} \\ -E_1 + iE_2 \end{Bmatrix} e^{i\alpha} \tag{41}$$

where n is outward unit normal at the boundary which also is represented, in complex form, by $e^{i\alpha}$ (where α defines the angle between the normal direction n and the positive x_1-axis). In the mapped plane, one can find the following relation from England (1971)

$$\alpha = \arg(\Omega'(\zeta)) + \eta, \qquad \zeta = \rho e^{i\eta} \tag{42}$$

3.5. Image force

The image force acting on the dislocation is an important physical quantity for understanding the interaction of a dislocation and inhomogeneities. The image force can be calculated by means of the generalized Peach-Koehler formula by Pak (1990).

$$\begin{aligned} F_1 &= b\tau_{32}^T + \Delta\phi D_2^T + p_0\gamma_{31}^T + q_0E_1^T \\ F_2 &= -b\tau_{31}^T - \Delta\phi D_1^T + p_0\gamma_{32}^T + q_0E_2^T \end{aligned} \tag{43}$$

where τ_{31}^T, τ_{32}^T, γ_{31}^T, γ_{32}^T, D_1^T and D_2^T are the perturbation shear stress, shear strain and electric displacement components at the dislocation. Substituting Eqs. (38) and (39) into Eq.(43) gives

$$F_1 - iF_2 = \begin{Bmatrix} c_{44}^c bi + e_{15}^c\Delta\phi i + p_0 \\ e_{15}^c bi - \varepsilon_{11}^c\Delta\phi i - q_0 \end{Bmatrix}^T \frac{-\sum_{n=1}^{\infty} n\mathbf{c}_{-n}\zeta^{-n-1}}{R\left(1 - \sum_{n=1}^{\infty} m_n n\zeta^{-n-1}\right)} \tag{44}$$

4. Numerical results

In the following discussion, the core inclusion and the unbounded matrix are assumed to be made up of PZT-5H with material constants $c_{44} = 35.3GNm^{-2}$, $\varepsilon_{11} = 15.1nCV^{-1}m^{-1}$, $e_{15} = 17Cm^{-2}$ and the interphase layer is made up of PZT-7A with material constants $c_{44} = 25.4GNm^{-2}$, $\varepsilon_{11} = 4.071nCV^{-1}m^{-1}$, $e_{15} = 9.2Cm^{-2}$. When the matrix is subjected to a point loading ($p_0 = 5MN/m$, $q_0 = 10^{-3}C/m$) located at $z_0 = 2i$, Figs. 3-6 respectively show the normal shears along the interfaces of various shaped inclusions. Figs. 7-10 respectively show the tangential electric fields along the interfaces of various shaped inclusions. It is obvious that the magnitudes of the interfacial normal shear and tangential electric field in the upper plane (x_2>0) are lager than those in the lower plane (x_2<0), since the point force is applied at $z_0 = 2i$. The maximum values of $\tau_{3n}R/p_0$ and $E_t R\varepsilon_{11}^c/q_0$ are listed in Table 1. Furthermore, we will investigate the effects of material constant combinations on the image force. The unbounded matrix is also assumed to be PZT-5H and the screw dislocation with Burgers vector $b_z = 10^{-9}m$ and electric potential jump $\Delta\phi = 1.0V$ located at the point of the positive x_1-axis. We first check the case of three-phase circular inclusion problem that is the special case of $m_n = 0$ in Eq. 13. Figure 11 shows the variations of the image force with respect to the position of the dislocation for various elastic modulus of the interphase layer. Figure 12 shows the variations of the image force with respect to the position of the dislocation for various thicknesses of the interphase layer. These results are in agreement with those of Liu et al. (2004). Figures 13 and 14 show the variations of image force for various elastic modulus of the interphase layer. Fig. 15 shows the variations of image force for piezoelectric constant of the interphase layer. In these cases, the thickness of the interphase layer in the mapped plane is assumed to be 0.1. The positive image force represents the coated inclusion will repel the piezoelectric screw dislocation in the matrix and the negative image force represents the coated inclusion will attract the piezoelectric screw dislocation in the matrix. It can be observed that the coated inclusion will repel the piezoelectric screw dislocation in the matrix (positive image force) for $c_{44}^b > c_{44}^c$ or $e_{15}^b > e_{15}^c$ and will attract the piezoelectric screw dislocation in the matrix (negative image force) for $c_{44}^b < c_{44}^c$ or $e_{15}^b < e_{15}^c$ when the dislocation is near to the interface.

5. Conclusion

The problem of a piezoelectric screw dislocation in an arbitrarily shaped three-phase composite is analyzed in the framework of linear piezoelectricity. Based on the methods of complex variable, conformal mapping, Faber series and Laurent series, the analytical complex potentials are derived in series form. Once the complex potentials are determined, the stress, electric field and image force can be expressed explicitly. The numerical results indicate that the mismatch of material constants and the shapes of the inclusions have significant effects on the shear stress, electric field and the Peach-Koehler force. These results can be used to increase the performance of the piezoelectric sensor and to protect the vulnerable piezoelectric ceramics from mechanical damage in a piezoelectric composite material system. Besides, some specific examples are provided and verified to be consistent with the existing ones.

References

Barnett, D.M., Lothe, J., 1975. Dislocations and line charges in anisotropic piezoelectric insulators. Physica Status Solidi B 67, 105-111.

Chao, C.K., Chang,K.J., 1999. Interacting circular inclusions in antiplane piezoelectricity. International Journal of Solids and Structures 36, 3349-3373.

Deng, W., Meguid, S.A., 1999. Analysis of a screw dislocation inside an elliptical inhomogeneity in piezoelectric solids. International Journal of Solids and Structures 36, 1449-1469.

England, A.H., 1971. Complex Variable Methods in Elasticity. Wiley-Interscience, London.

Gao, C.F. Noda, N., 2004. Faber series method for two-dimensional problems of arbitrarily shaped inclusion in piezoelectric materials. Acta Mechanica 171, 1-13.

Gdoutos, E.E, Kattis, M.A., 1990. Partially bonded rigid round-off corners polygonal inclusions in an elastic matrix. International Journal of Fracture 43, 133-159.

Huang, Z., Kuang, Z.B., 2001. Dislocation inside a piezoelectric media with an elliptical inhomogeneity. International Journal of Solids and Structures 38, 8459-8480.

Jiang, C. P., Cheung, Y. K., 2001. An exact solution for the three-phase piezoelectric cylinder model under antiplane shear and its applications to piezoelectric composites. International Journal of Solids and Structures 38, 4777-4796.

Jiang, C.P. Tong, Z.H., Cheung, Y.K., 2001. A generalized self-consistent method for piezoelectric fiber reinforced composites under antiplane shear. Mechanics of Materials 33, 295-308.

Kattis, M.A., Providas, E., Kalamkarov, A.L., 1998. Two-phase potentials in the analysis of smart composites having piezoelectric components. Composites Part B: Engineering 29, 9-14.

Kosevich, A.M., Pastur, L.A., Feldman, E.P., 1968. Dislocation and linear charge fields in piezoelectric crystals. Soviet Physics Crystallography 12, 797–801.

Lee, K.Y., Lee, W.G., Pak, Y. E., 2000. Interaction between a semi-infinite crack and a screw dislocation in a piezoelectric material. Journal of Applied Mechanics-Transactions of the ASME 67, 165-170.

Liu, Y.W., Fang, Q.H., Jiang, C.P., 2004. A piezoelectric screw dislocation interacting with an interphase layer between a circular inclusion and the matrix. International Journal of Solids and Structures 41, 3255-3274.

Meguid, S.A., Deng, W., 1998. Electro-elastic interaction between a screw dislocation and elliptical inho\mogeneity in piezoelectric materials. International Journal of Solids and Structures 35, 1467-1482.

Meguid, S.A., Zhong, Z., 1998. On the elliptical inhomogeneity problem in piezoelectric materials under antiplane shear and inplane electric field. International Journal of Engineering Science 36, 329-344.

Nowacki, J.P., Alshits, V.I., 2007. Dislocation fields in piezoelectrics, in: Dislocations in Solids. vol. 13, Eds. F.R.N. Nabarro, J.P. Hirth, Elsevier, Amsterdam, 47-79.

Pak, Y.K., 1990. Force on a Piezoelectric Screw Dislocation. Journal of Applied Mechanics-Transactions of the ASME 57, 165-170.

Pak, Y.E., 1992. Circular inclusion problem in anti-plane piezoelectricity. International Journal of Solids and Structures 29, 2403–2419.

Pengfei, H., Ishikawa, H., Kohno, H., 1995. Analysis of the orders of stress singularity at the corner point of a diamond-shape rigid inclusion or hole in an infinite plate under antiplane bending by conformal mapping. International Journal of Engineering Science 33, 1535-1546.
Ru, C.Q., 1999. Analytical solution for Eshelby's problem of an inclusion of arbitrary shape in a plane or half-plane. Journal of Applied Mechanics-Transactions of the ASME 66, 315-322
Ru, C.Q., 2000. Eshelby's problem for two-dimensional piezoelectric inclusions of arbitrary shape. Proceedings of the Royal Society A456, 1051-1068.
Saada G., 1971. Dislocations dans lex cristaux piezoelectriques. Physica Status Solidi B 44, 717-731.
Shen, M. H., Chen, F. M, Chen, S. N., Hung, S. Y., 2009. Piezoelectric study for a coated hole of quasi-polygonal shape in an infinite plate. International Journal of Engineering Science 47, 475-486.
Sudak, L.J., 2003. Effect of an interphase layer on the electroelastic stresses within a three-phase elliptic inclusion. International Journal of Engineering Science 41, 1019-1039.
Wang, X., Shen, Y.P., 2003. Inclusions of arbitrary shape in magnetoelectroelastic composite materials. International Journal of Engineering Science 41, 85-102.
Wang, X., Sudak, L.J., 2006. Interaction of a screw dislocation with an arbitrary shaped elastic inhomogeneity. Journal of Applied Mechanics-Transactions of the ASME 73, 206-211.
Zhang, T.Y., Tong, P., 1996. Fracture mechanics for a mode Ⅲ crack in a piezoelectric material. International Journal of Solids and Structures 33, 343-359.

Table 1. The maximum values of normal shear and tangential electric field in Figs. 3-10

		$\tau_{3n}R/p_0$		$E_t\, R\varepsilon_{11}^c/q_0$	
Shapes of inclusions and Mapping function constants		Maximum value	Position	Maximum value	Position
Shape 1 $m_2=-0.2,\ m_3=-0.1$	Inner interface	0.2331	$\psi=84^\circ$	-0.6343 0.4589	$\psi=50^\circ$ $\psi=146^\circ$
	Outer interface	0.2517	$\psi=87^\circ$	-1.0653 0.6419	$\psi=53^\circ$ $\psi=131^\circ$
Shape 2 $m_3=-0.15,\ m_7=-0.07$	Inner interface	0.2161	$\psi=69^\circ$	-0.6465 0.6465	$\psi=55^\circ$ $\psi=125^\circ$
	Outer interface	0.2470	$\psi=90^\circ$	-0.8598 0.8598	$\psi=64^\circ$ $\psi=116^\circ$
Shape 3 $m_2=-0.2,\ m_5=-0.1$	Inner interface	0.3001	$\psi=80^\circ$	-0.7284 0.6353	$\psi=72^\circ$ $\psi=98^\circ$
	Outer interface	0.2665	$\psi=87^\circ$	-0.9332 0.7323	$\psi=38^\circ$ $\psi=153^\circ$
Shape 4 $m_1=1/2,\ m_3=-1/8,\ m_5=-3/80,$ $m_7=-3/896,\ m_9=5/768,$ $m_{11}=57/11264$	Inner interface	0.1625	$\psi=90^\circ$	-0.3749 0.3749	$\psi=30^\circ$ $\psi=150^\circ$
	Outer interface	0.1736	$\psi=90^\circ$	-0.7939 0.7939	$\psi=30^\circ$ $\psi=150^\circ$

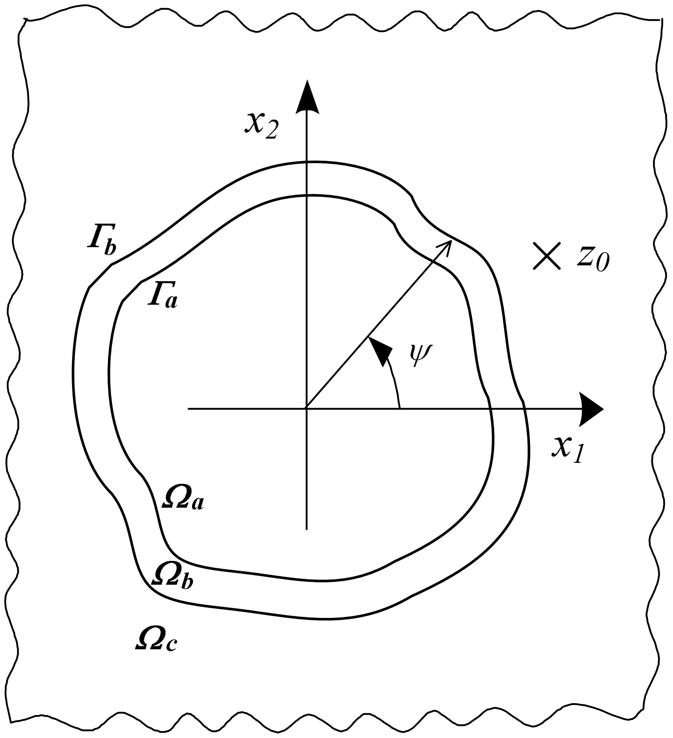

Fig. 1. A screw dislocation in an arbitrarily shaped three-phase piezoelectric composite.

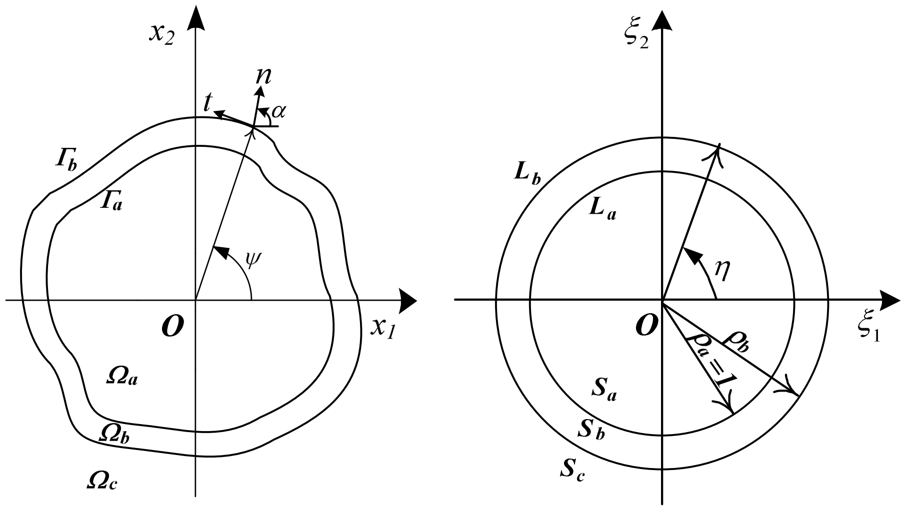

Fig. 2. The conformal mapping from z-plane to ζ-plane.

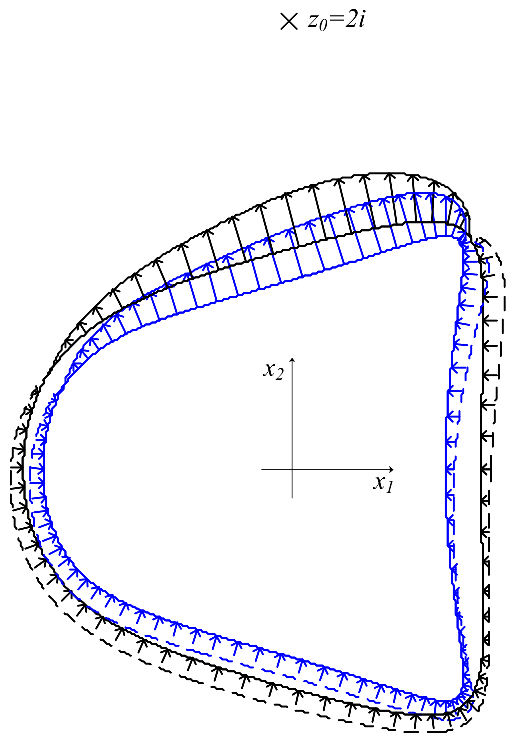

Fig. 3. The normal shear $\tau_{3n}R/p_0$ along the interfaces of inclusion (shape 1).

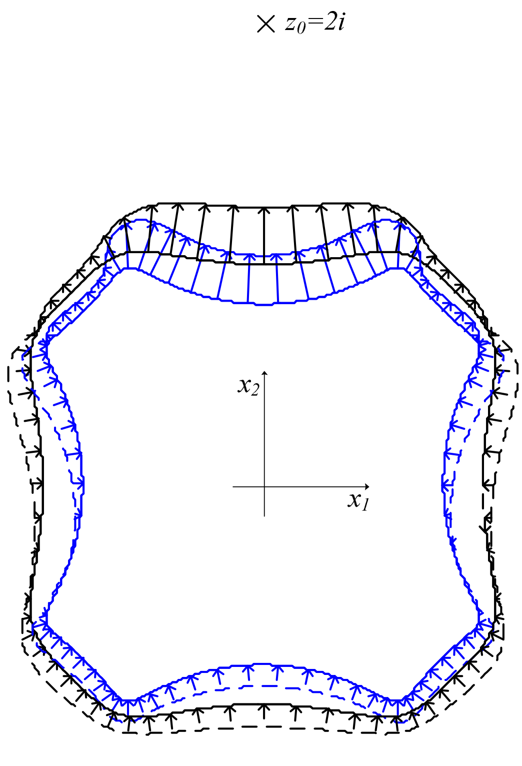

Fig. 4. The normal shear $\tau_{3n}R/p_0$ along the interfaces of inclusion (shape 2).

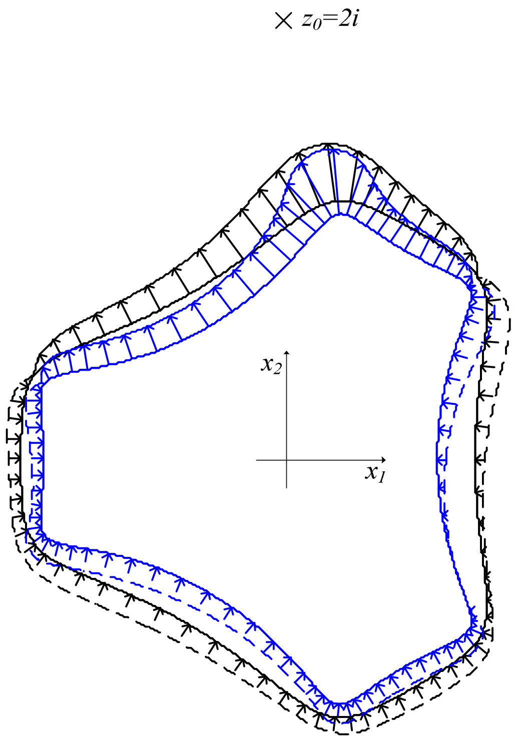

Fig. 5. The normal shears $\tau_{3n} R / p_0$ along the interfaces of inclusion (shape 3).

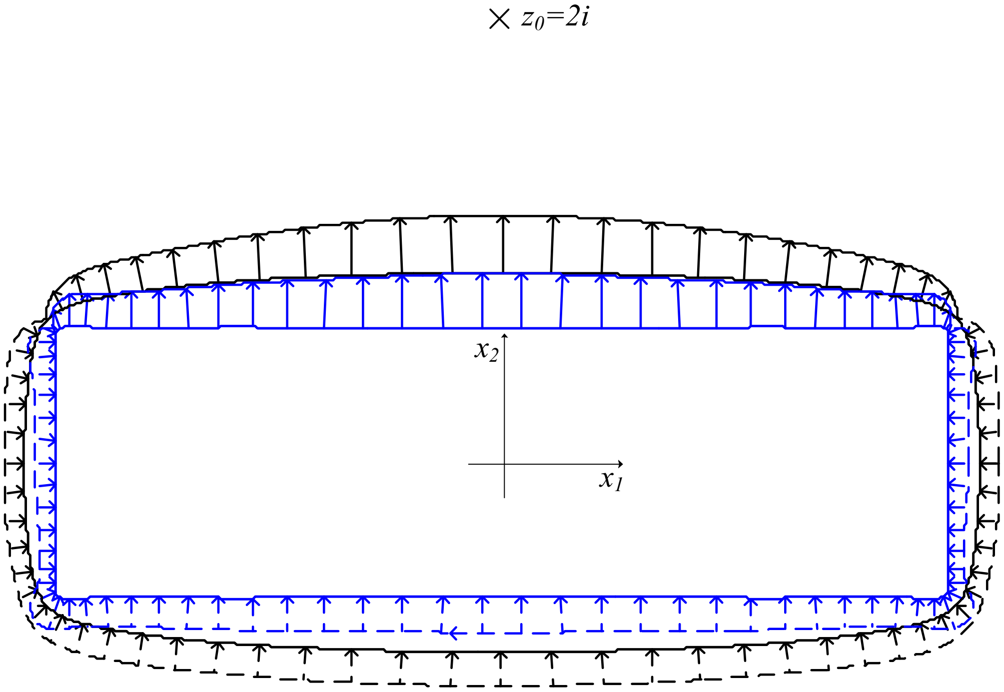

Fig. 6. The normal shear $\tau_{3n} R / p_0$ along the interfaces of inclusion (shape 4).

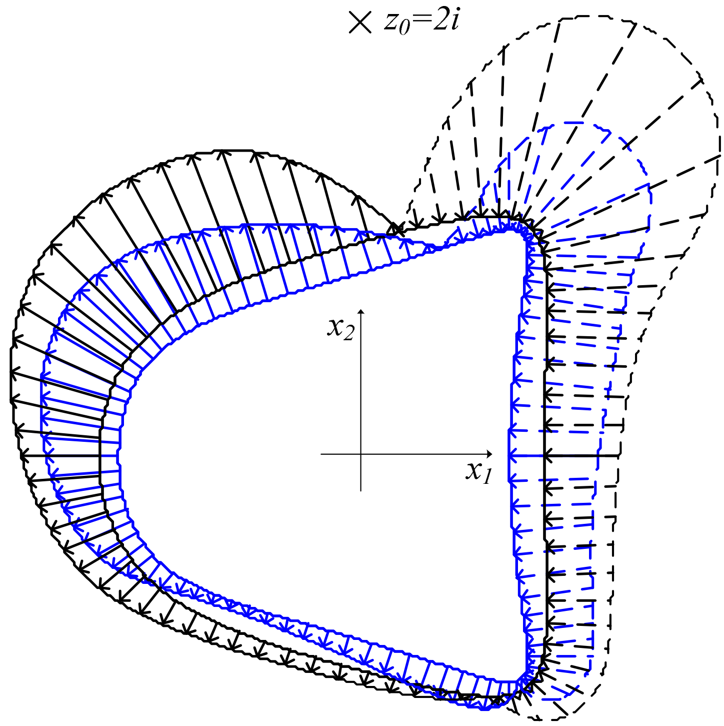

Fig. 7. The tangential electric field $E_t\, R\varepsilon_{11}^c / q_0$ along the interfaces of inclusion (shape 1).

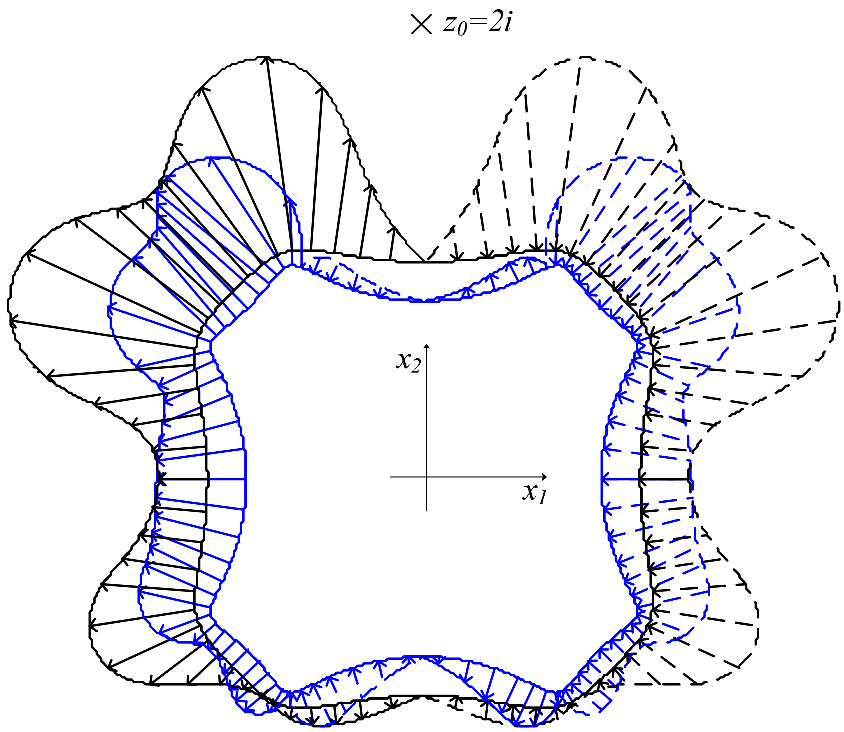

Fig. 8. The tangential electric field $E_t\, R\varepsilon_{11}^c / q_0$ along the interfaces of inclusion (shape 2).

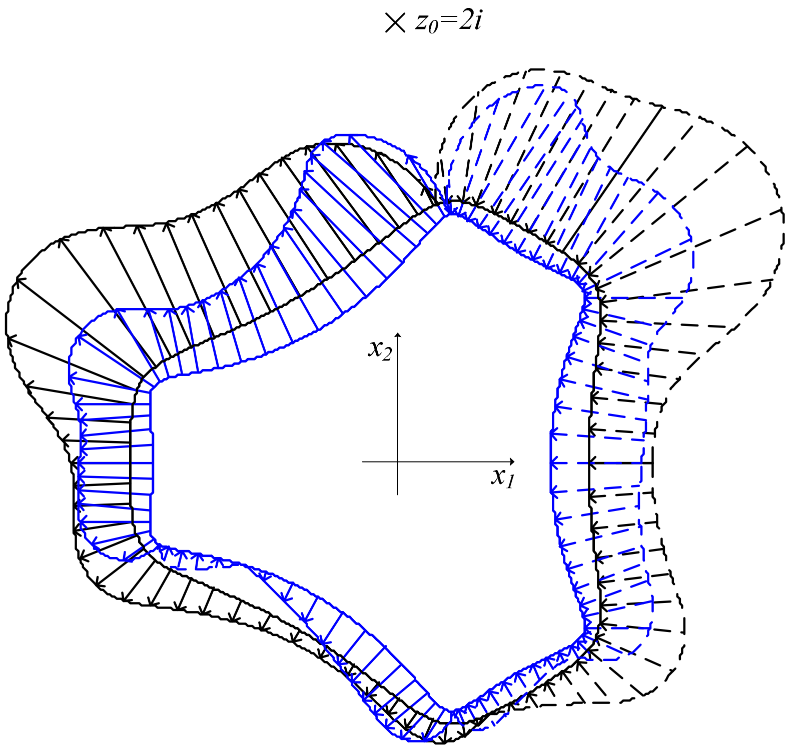

Fig. 9. The tangential electric field $E_t\, R\varepsilon_{11}^c / q_0$ along the interfaces of inclusion (shape 3).

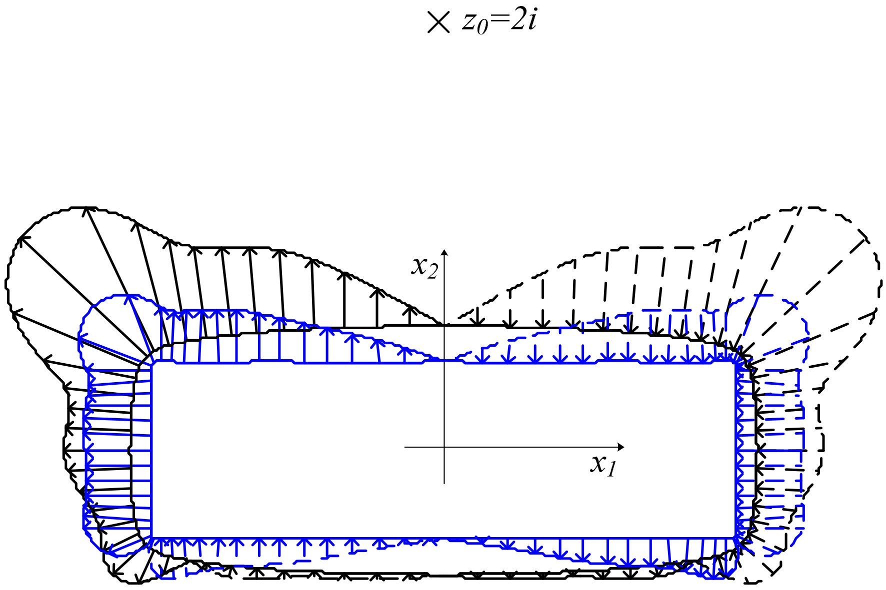

Fig. 10. The tangential electric field $E_t\, R\varepsilon_{11}^c / q_0$ along the interfaces of inclusion (shape 4).

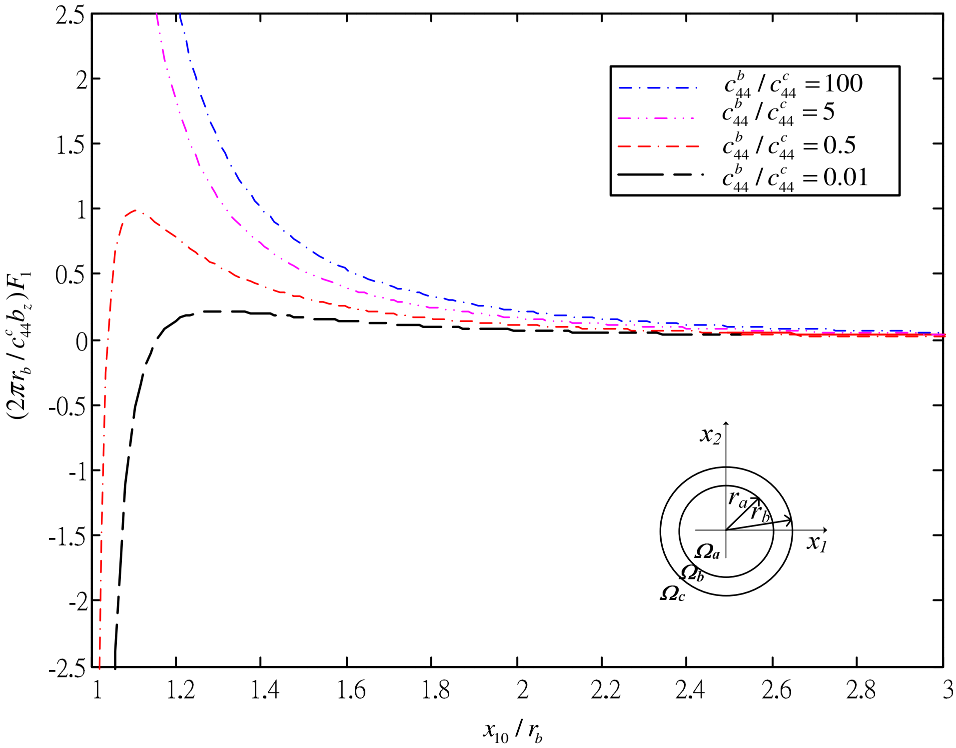

Fig. 11. The variations of image force with respect to the position of the dislocation for various elastic modulus of the interphase layer ($r_a = 0.9 r_b$, $\mathbf{C}_a = 5\mathbf{C}_c$, $e_{15}^b = e_{15}^c$, $\varepsilon_{11}^b = \varepsilon_{11}^c$).

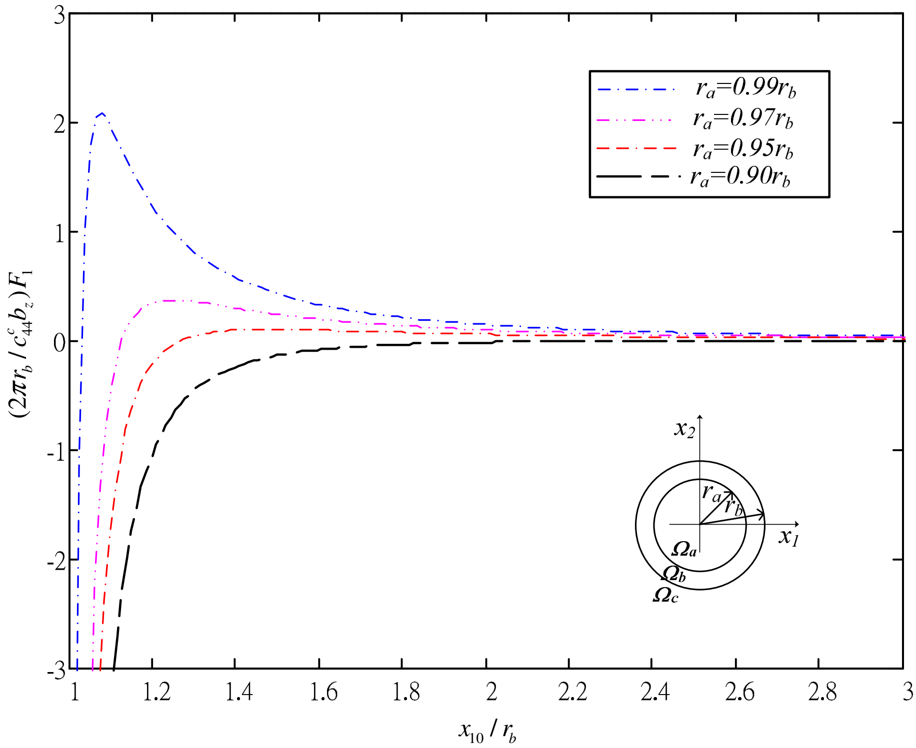

Fig. 12. The variations of image force with respect to the position of the dislocation for various thicknesses of the interphase layer ($\mathbf{C}_a = 5\mathbf{C}_c$, $c_{44}^b = 0.2 c_{44}^c$, $e_{15}^b = 0.2 e_{15}^c$, $\varepsilon_{11}^b = \varepsilon_{11}^c$).

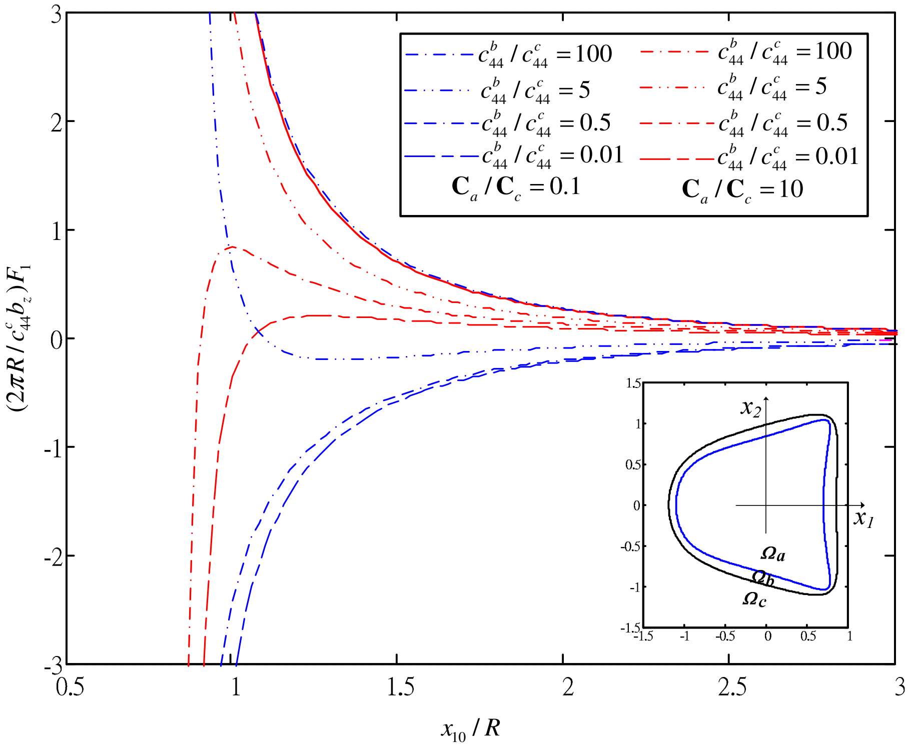

Fig. 13. The variations of image force with respect to the position of the dislocation for various elastic modulus of the interphase layer ($\rho_b = 1.1$, $e_{15}^b = e_{15}^c$, $\varepsilon_{11}^b = \varepsilon_{11}^c$, shape 1).

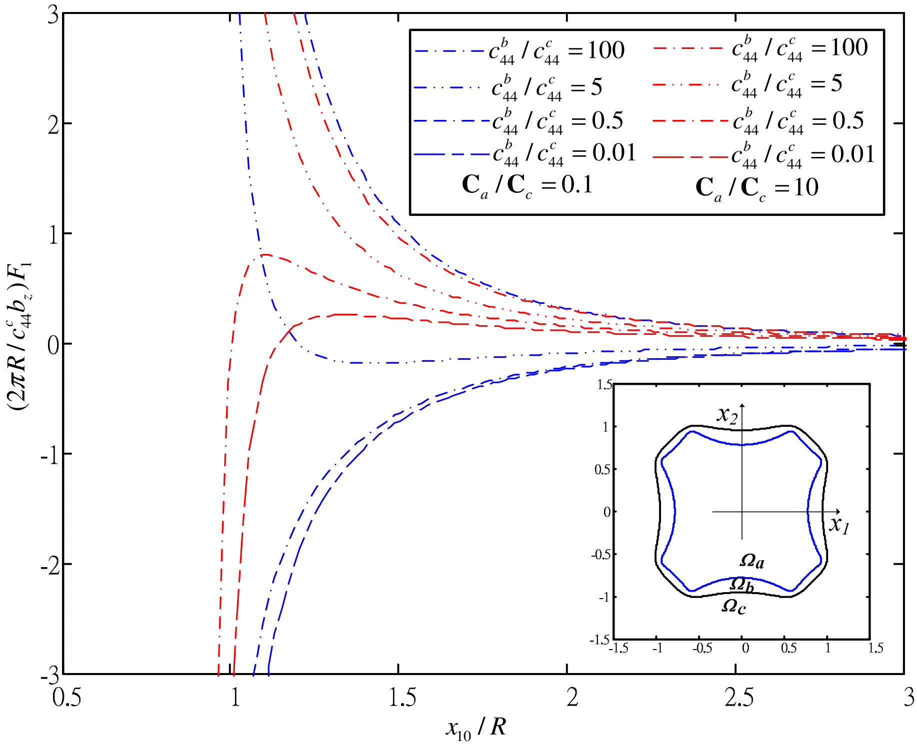

Fig. 14. The variations of image force with respect to the position of the dislocation for various elastic modulus of the interphase layer ($\rho_b = 1.1$, $e_{15}^b = e_{15}^c$, $\varepsilon_{11}^b = \varepsilon_{11}^c$, shape 2).

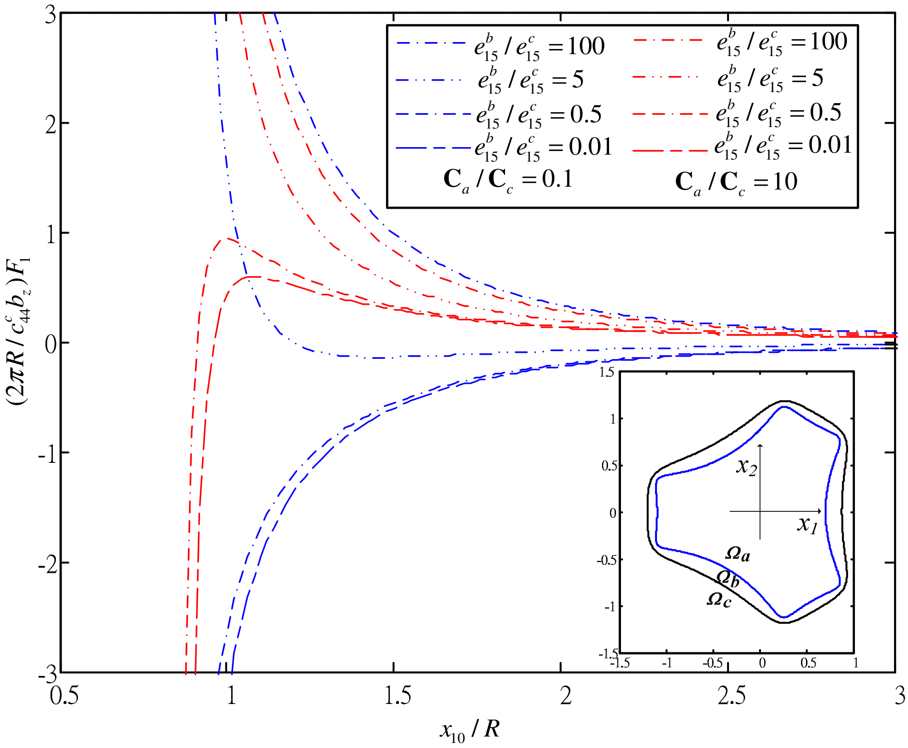

Fig. 15. The variations of image force with respect to the position of the dislocation for various elastic modulus of the interphase layer ($\rho_b=1.1$, $c_{44}^b=c_{44}^c$, $\varepsilon_{11}^b=\varepsilon_{11}^c$, shape 3).